Two-Dimensional Crystallization of Ca-ATPase by Detergent Removal

Jean-Jacques Lacapère,* David L. Stokes,# Anders Olofsson,* and Jean-Louis Rigaud*
*Institut Curie, Section de Recherche, UMR-CNRS 168, LRC-CEA 8, 75005 Paris Cedex, France, and #Skirball Institute for Biomolecular Medicine, New York University Medical Center, New York, New York 10016 USA

ABSTRACT By using Bio-Beads as a detergent-removing agent, it has been possible to produce detergent-depleted two-dimensional crystals of purified Ca-ATPase. The crystallinity and morphology of these different crystals were analyzed by electron microscopy under different experimental conditions. A lipid-to-protein ratio below 0.4 w/w was required for crystal formation. The rate of detergent removal critically affected crystal morphology, and large multilamellar crystalline sheets or wide unilamellar tubes were generated upon slow or fast detergent removal, respectively. Electron crystallographic analysis indicated unit cell parameters of $a = 159$ Å, $b = 54$ Å, and $\gamma = 90°$ for both types of crystals, and projection maps at 15-Å resolution were consistent with Ca-ATPase molecules alternately facing the two sides of the membrane. Crystal formation was also affected by the protein conformation. Indeed, tubular and multilamellar crystals both required the presence of Ca^{2+}; the presence of ADP gave rise to another type of packing within the unit cell ($a = 86$ Å, $b = 77$ Å, and $\gamma = 90°$), while maintaining a bipolar orientation of the molecules within the bilayer. All of the results are discussed in terms of nucleation and crystal growth, and a model of crystallogenesis is proposed that may be generally true for asymmetrical proteins with a large hydrophilic cytoplasmic domain.

INTRODUCTION

P-type ion pumps comprise a subfamily of ion transport ATPases and are named for the covalent phosphoenzyme formed as part of the transport cycle catalyzed by these proteins. Proteins of this subfamily share both amino acid homology and a basic reaction mechanism (Lutsenko and Kaplan, 1995). The Ca-ATPase of sarcoplasmic reticulum is one of the best known members of this P-type ATPase subfamily. Detailed information on the transport cycle has been provided (Møller et al., 1996), and functional studies have clearly shown a vectorial calcium/proton countertransport at the expense of ATP hydrolysis (Levy et al., 1990c; Hao et al., 1994).

Although we have a lot of information concerning the topology and topography of these proteins through biochemical, biophysical, and molecular biological studies, no P-type pump structure has yet been solved at atomic resolution (Stokes, 1991). In this context, electron microscopic studies of two-dimensional crystals (2D) of Ca-ATPase have led to important information, but at limited resolution. Indeed, two different crystal forms have been produced: 1) tubular crystals induced by the addition of vanadate, calcium, or lanthanide to SR vesicles (Dux and Martonosi, 1983; Dux et al., 1985) or the addition of vanadate to reconstituted proteoliposomes (Young et al., 1997); 2) large, flat, multilamellar crystals grown from detergent-solubilized SR (Dux et al., 1987; Stokes and Green, 1990a). However, three-dimensional reconstruction of the vanadate-induced tubes (Toyoshima et al., 1993; Yonekura et al., 1997; Zhang et al., 1998) has only recently provided 8-Å resolution because of the low signal-to-noise ratio from these relatively small crystals. In the case of the large flat crystals grown in the presence of detergent, projection maps at 6-Å resolution have been calculated (Stokes and Green, 1990b). Although diffraction extends up to much higher resolution (3.5 Å), three-dimensional reconstruction is complicated by the multilayer structure of the crystals (Misra et al., 1991; Varga et al., 1991; Shi et al., 1995). From all of these considerations, there is clearly a need to develop new strategies and to understand the mechanisms underlying 2D crystal formation of P-type ATPases to produce new 2D crystals suitable for higher resolution structural analysis.

In the present work we have developed a strategy for producing novel 2D crystals from purified Ca-ATPase. Basically, we extended our previous reconstitution studies (Levy et al., 1992; Rigaud et al., 1995; Young et al., 1997) to include 2D crystallization of Ca-ATPase at very low lipid-to-protein ratios. Two-dimensional crystals were generated by complete detergent removal from micellar lipid-protein-detergent mixtures by using Bio-Beads SM2 (Rigaud et al., 1997; 1998). In particular, the rate of detergent removal was crucial in determining the morphology of 2D crystals, which appeared either as unilamellar tubes or as multilayered crystals. The protein conformation was also important because the removal of calcium ions disrupted the preformed 2D crystals, and the presence of ADP gave rise to a novel 2D crystal form. Electron crystallography showed that all 2D crystals with low lipid-to-protein ratios comprised proteins arranged, alternately, up and down within the membrane. Based on these observations, we propose that the symmetrical packing of the proteins is controlled by the lipid-to-protein ratio, whereas crystal growth and final morphology are controlled by the rate of detergent removal.

Received for publication 29 January 1998 and in final form 27 May 1998.
Address reprint requests to Dr. Jean-Jacques Lacapère, Institut Curie, Section de Recherche, UMR-CNRS 168, LRC-CEA 8, 11 rue Pierre et Marie Curie, 75005 Paris Cedex, France. Tel.: 33-1-42-34-67-81; Fax: 33-01-40-51-06-36; E-mail: lacapere@curie.fr.

0006-3495/98/09/1319/11 $2.00

MATERIALS AND METHODS

Materials

Purified egg yolk phosphatidylcholine (EPC) and egg yolk phosphatidic acid (EPA) were purchased from Avanti Polar Lipids. Octaethylene glycol mono-*n*-1-dodecyl ether ($C_{12}E_8$) was from Nikko Chemical (Tokyo, Japan), and the radioactively labeled derivative was from Saclay, France; Bio-Beads SM2 (25–50 mesh) were purchased from Bio-Rad. All other reagents were of analytical grade.

Preparation of Ca-ATPase

Sarcoplasmic reticulum vesicles were prepared as described by Champeil et al. (1985). Ca-ATPase was purified by Reactive Red affinity chromatography, as described by Stokes and Green (1990a): briefly, sarcoplasmic reticulum, solubilized at 2 mg/ml in 10 mg/ml $C_{12}E_8$, was bound to a Reactive Red affinity column and eluted with a buffer containing 1 mg/ml $C_{12}E_8$, 1 mM $CaCl_2$, 1 mM $MgCl_2$, 20 mM 3-(*N*-morpholino)propanesulfonic acid-KOH (MOPS-KOH) (pH 7), 20% glycerol, 0.25 mM dithiothreitol, and 2–4 mM ADP. The fractions with both the highest protein concentration (~2 mg protein/ml) and ATPase activity (6–8 μmol ATP/mg min) were pooled, frozen in liquid nitrogen, and used for further crystallization trials.

Lipid determination

The amount of lipids present both in the sarcoplasmic reticulum vesicles and in the purified ATPase preparations was determined (see Table 1) according to the procedure described by Rouser et al. (1970). Briefly, the lipids were digested with perchloric acid by heating at 200°C for 2 h, and the total phosphorus in the samples was determined against a calibration curve done with disodium hydrogen phosphate after a phosphomolybdate complex was formed.

Crystallization

The purified preparation of Ca-ATPase was resuspended at 0.2 mg/ml in 100 mM KCl, 0.1 mM $CaCl_2$, 1 mg/ml $C_{12}E_8$, 10 mM MOPS-KOH (pH 7), and supplemented with the desired amount of EPC-EPA (9/1 M/M). $C_{12}E_8$ was removed by hydrophobic adsorption onto Bio-Beads SM2 as described in the Results.

Electron microscopy

For negative staining, 5 μl of the reconstituted samples (0.2 mg of protein/ml) was applied to carbon-coated grids, blotted, and stained with 1% uranyl acetate. The specimens were viewed with a Philips CM120 electron microscope operating at 120-kV accelerating voltage.

Image analysis

Micrographs were screened by optical diffraction, and a subset of images showing sharp diffraction spots was selected for computer processing. These images were digitized on a Leafscan 45 microdensitometer at 10–45-μm intervals, depending on plate magnification, with a constant step size of 5 Å on the film. Digitized micrographs were processed with MRC programs to correct the distortion of the crystal lattice (Henderson et al., 1986). Space group determination was made with the ALLSPACE program (Valpuesta et al., 1994). Projection maps were calculated from data with or without imposed symmetry, and finally from merged data averaged for *c*12 symmetry.

TABLE 1 Lipid content of Ca-ATPase preparations

Preparation	Lipid/protein molar ratio	Lipid/protein weight ratio*
Sarcoplasmic reticulum vesicles	80–100	0.5–0.7 mg/mg
Purified Ca-ATPase	6–8	0.04–0.05 mg/mg

*Assuming PM = 115.000 for the Ca-ATPase and an average value of 800 for lipids.

RESULTS

Production of 2D crystals with Bio-Beads SM2 as the detergent removing agent

Two-dimensional Ca-ATPase crystals were obtained from micellar solutions containing $C_{12}E_8$, purified Ca-ATPase, and phospholipids (EPC-EPA, 9/1 M/M) at lipid-to-protein ratios lower than 0.4 w/w. Then detergent was removed by hydrophobic adsorption onto Bio-Beads SM2. This strategy allows the removal of almost all of this low critical micelle concentration detergent in a relatively short time (Levy et al., 1990b,c). Also important for this sudy, it provides control over the rate of detergent removal by controlling the amount of beads, allowing the analysis of kinetic factors involved in crystallogenesis (Young et al., 1997; Rigaud et al., 1997). To ensure complete detergent removal, an excess of Bio-Beads (above the determined adsorptive capacity of 0.2 g $C_{12}E_8$/g of wet beads) was added directly to the micellar solutions. Fast detergent removal corresponded to the addition of this amount of beads at once, and slow or intermediate rates of detergent removal corresponded to successive additions of small numbers of beads at desired time intervals. For our crystallization conditions, $C_{12}E_8$ was completely removed in 30 min or 2 h, which we refer to as fast and slow rates, respectively (Fig. 1). No major lipid or protein loss occurred during detergent removal (data not shown; see also Rigaud et al., 1997).

Effect of the rate of detergent removal on the crystallization process

Slow rate of detergent removal

The structures formed upon slow detergent removal, at different lipid-to-protein ratios, were examined by electron microscopy after negative staining. Table 2 indicates that crystals are only produced at low lipid-to-protein ratios (0.1–0.35 w/w), slightly below the range of the 3D crystals formed in the presence of detergent (0.3–0.5 w/w; Taylor et al., 1988; Shi et al., 1995; Stokes and Green, 1990a), but well below the one observed in the native SR preparation (Table 1). Within this narrow range, the largest crystals were produced at the highest lipid-to-protein ratios.

Fig. 2 shows typical electron micrographs with our schematic interpretation on the right side. In the absence of added lipids (i.e., at a lipid/protein ratio = 0.05 w/w, taking into account the endogenous lipid in the purified Ca-ATPase), some small monolayered crystals are observed (Fig. 2 *A*). After small amounts of lipids are added (final ratio of

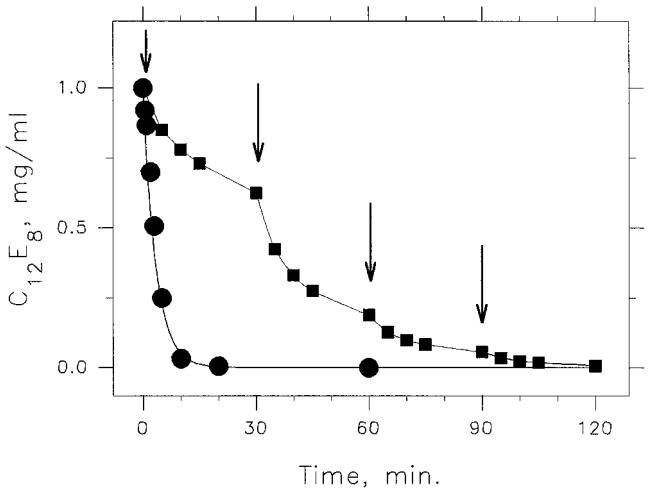

FIGURE 1 Kinetic of $C_{12}E_8$ removal upon Bio-Bead SM2 addition. Aliquots of 1-ml micellar lipid-detergent solutions containing 1 mg ^{14}C-$C_{12}E_8$/ml were treated by one addition of 40 mg beads/ml (●) or four successive additions of 2.5 mg beads/ml (■). This corresponds to fast and slow detergent removal, respectively. The beads were continuously stirred at room temperature, and aliquots from the supernatant were collected as a function of time and analyzed for their radioactivities.

0.1–0.15 w/w), a stacking of these small crystals is clearly observed, and "wormlike" crystals are formed (Fig. 2 *B*). These wormlike crystals consist of several (usually more than five) two-dimensional crystals stacked "in register"; within each layer, the hydrophilic domains of Ca-ATPase molecules protrude from both sides of the bilayer. Most of the crystals lie with the membrane plane perpendicular to the plane of the specimen support (see *scheme* in Fig. 2 *B*). For lipid-to-protein ratios between 0.2 and 0.3 w/w, these multilamellar crystals grow in the plane of the membrane, producing a platelike morphology. In this case, the membrane planes of these large multilamellar crystals (1.5 μm) are parallel to the plane of the specimen support (Fig. 2 *C*). Finally, for lipid-to-protein ratios above 0.4 w/w, closed vesicles with a dense protein packing are formed, but without observable crystallinity (Fig. 2 *D*).

A typical large multilamellar crystal is shown in Fig. 3 *A*, and its computed diffraction pattern appears in Fig. 3 *B*. The raw data exhibit diffraction spots to 20-Å resolution, and a centered lattice with parameters $a = 159 \pm 5$ Å, $b = 54 \pm 2$ Å, and $\gamma = 90 \pm 1°$ has been measured. Examination of the phase residual indicated a *c*12 two-sided plane group (Valpuesta et al., 1994) with twofold axes parallel to the *b* axis (see Table 4). We merged four images to get a 15-Å resolution projection map (Fig. 3 *C*). The molecules are aligned in rows, and according to the space group, proteins alternately protrude above and below the membrane.

Fast rate of detergent removal

Like slow detergent removal, crystallization by fast detergent removal occurred within a narrow range of lipid-to-protein ratios (see Tables 2 and 3), although no crystals were observed at the lowest lipid-to-protein ratio of 0.05 w/w. The main difference between fast and slow detergent removal is the crystal morphology.

Fig. 4 *A* shows that at a ratio of 0.1 w/w, stringlike lamellar aggregates are formed, with the large cytoplasmic domain of Ca-ATPase protruding from both surfaces (see *scheme* in Fig. 4 *A*). These strings are ~80 ± 20 nm long and contain 20–40 protein molecules. Increasing the lipid-to-protein ratio to 0.15 (w/w) generates twofold longer "strings," which tend to fold on one side, as shown in Fig. 4 *B*. At a lipid-to-protein ratio of 0.25 w/w, fast detergent removal induces the formation of wide tubular crystals, 0.2–0.5 μm long and 0.15–0.2 μm wide (Fig. 4 *C*). Finally, lipid-to-protein ratios above 0.4 w/w produce noncrystalline vesicles with a dense protein packing (Fig. 4 *D*).

The wide tubular crystals are novel and consist of either elongated vesicles or short opened vesicles. The tubular shape produces two overlapping crystal lattices, as seen in the broken tube in Fig. 5 *A*, where the lower edge of the membrane patch shows one lattice compared to the overlapping lattices in the rest of the membrane patch. The diffraction patterns are consistent with this analysis and show two reciprocal lattices with 20-Å resolution (Fig. 5 *B*). When considered individually, lattice parameters are $a = 158 \pm 6$ Å, $b = 54 \pm 5$ Å, and $\gamma = 90 \pm 3°$, which are similar to the lattice from multilayered crystals grown by slow detergent removal. The unit cell is orientated with the *a* axis oriented ~30° to the tube axis. It should be emphasized that these are likely to be helical crystals in solution, which have been flattened by negative staining.

Fifteen areas were selected by optical diffraction from nine of the best crystals and digitized. Examination of the phase residual indicated a *c*12 two-sided plane group (Valpuesta et al., 1994), as previously observed for the multilamellar crystals (see Table 4). A projection map was calculated at 15-Å resolution which closely resembles that of multilatered crystals showing molecules aligned along rows with a bipolar orintation (Fig. 5 *C*).

TABLE 2 Crystallization results upon slow rate of detergent removal

	Small unilayered crystals	Wormlike crystals	Platelike crystals	Large platelike crystals	Large platelike crystals	Vesicles	Vesicles	Vesicles
Final lipid-to-protein ratio by weight	0.05	0.10	0.15	0.20	0.25	0.45	0.85	1.85

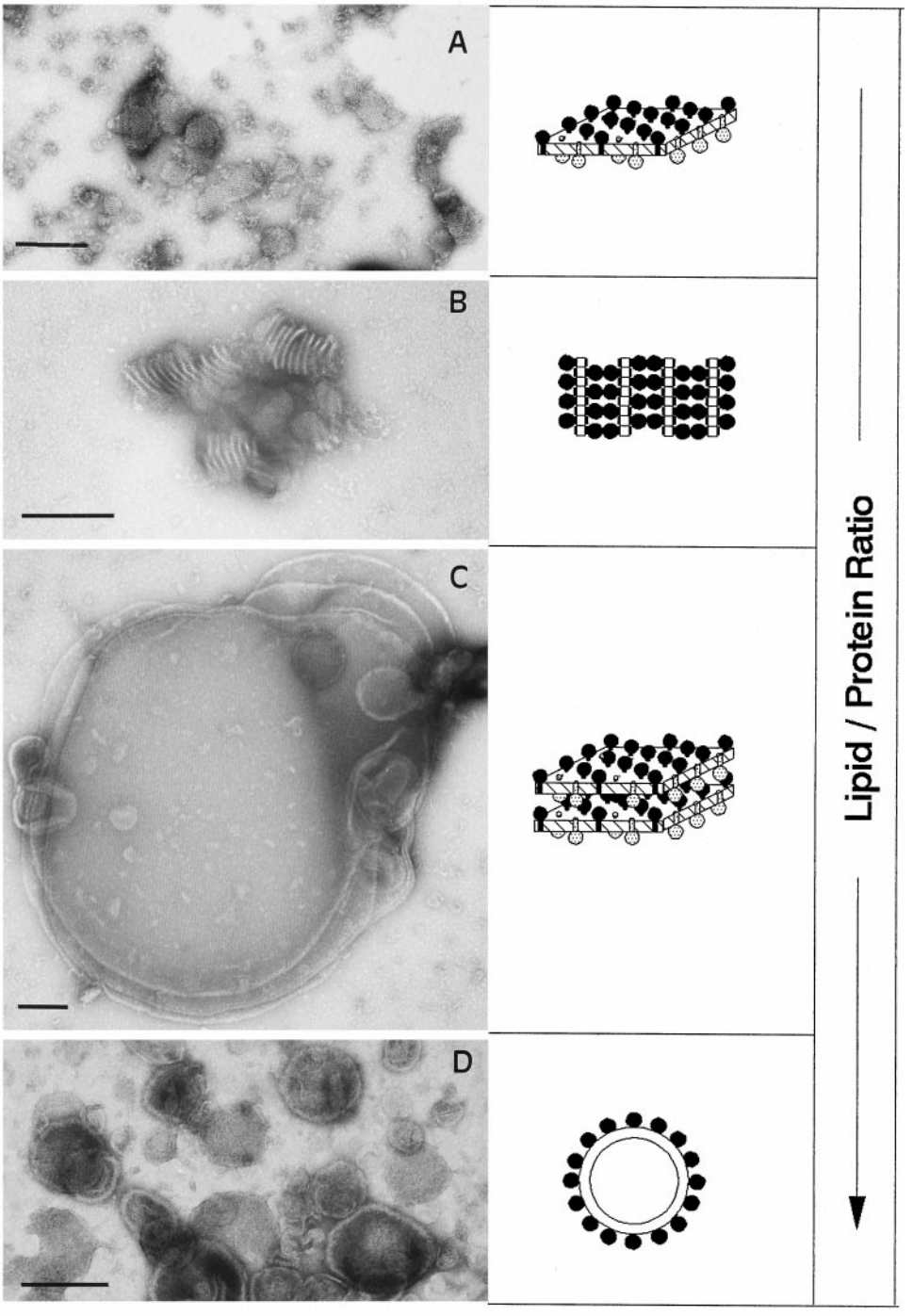

FIGURE 2 Effect of lipid-to-protein ratio on Ca-ATPase crystallization induced by slow rate of detergent removal. For crystallization, the purified $C_{12}E_8$-solubilized Ca-ATPase was resuspended at 0.2 mg/ml in 100 mM KCl, 0.1 mM $CaCl_2$, 1 mg/ml $C_{12}E_8$, 10 mM MOPS-KOH (pH 7), and supplemented with the desired amount of EPC-EPA (9/1). $C_{12}E_8$ was removed by four successive additions of beads at a beads/detergent ratio of 10 w/w, corresponding to slow detergent removal as described in Fig. 1. After detergent removal, the structures formed were analyzed by negative staining. Electron micrographs of samples reconstituted at different lipid-to-protein ratios: (*A*) No added lipids, i.e., at a lipid/protein ratio = 0.05 w/w, taking into account the endogenous lipid in the purified Ca-ATPase. (*B*) Addition of 0.05 mg lipids per mg protein, i.e., final lipid/protein ratio = 0.1 w/w. (*C*) Addition of 0.15 mg lipids per mg protein, i.e., final lipid/protein = 0.2 w/w. (*D*) Addition of 0.80 mg lipids per mg protein, i.e., final lipid/protein ratio = 0.85 w/w. Schematic interpretations of the different structures are shown on the right side. The scale bar represents 200 nm.

Crystal formation during detergent removal

Two-dimensional crystal formation has been followed by analysis of the structures formed during slow detergent removal (data not shown). In the starting solution, electron micrographs show small "aggregates" characteristic of lipid–detergent–Ca-ATPase micelles. At the very beginning of detergent removal, these aggregates fuse and small unilamellar crystals appear, and these progressively grow into large multilayered crystals. Once the detergent has been totally removed, the size, morphology, and order of the multilayered 2D crystals do not evolve upon incubation for many days.

Thus it appears that 2D crystals of Ca-ATPase form at the very beginning of the micellar-to-lamellar transition. This observation is consistent with that of Dolder et al. (1996), who demonstrate that the micelle-to-vesicle transition is the critical step in the 2D crystallization. Our observations also suggest that stacking of 2D planar crystals into multilayered structures only occurs in the presence of detergent. Such an interpretation is corroborated by two other experimental observations. First, we found that slower detergent removal,

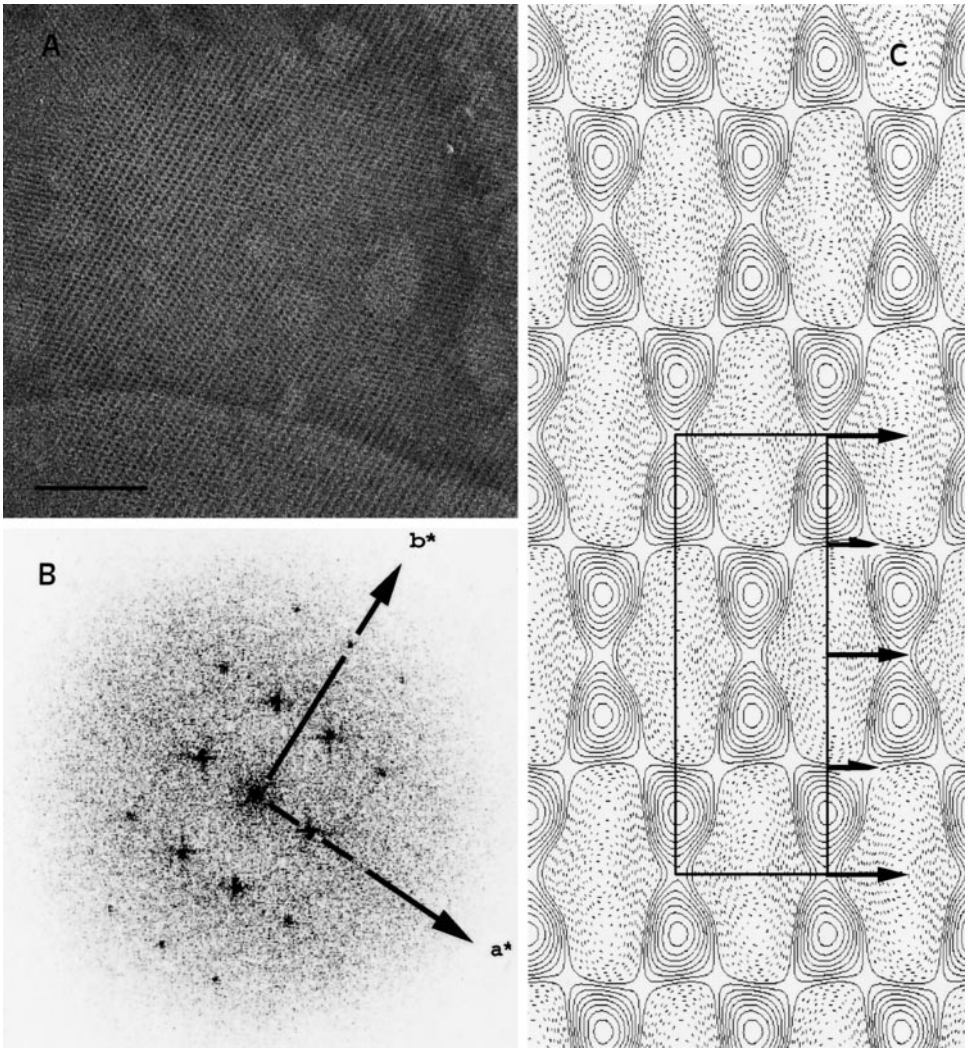

FIGURE 3 Image analysis of multilamellar Ca-ATPase crystals produced by slow rate of detergent removal. (*A*) Negatively stained Ca-ATPase crystals (lipid/protein = 0.2 w/w) recorded at high magnification. Scale bars represent 100 nm. (*B*) Computed diffraction pattern of multilamellar Ca-ATPase crystals. (*C*) Projection map of multilayered crystals obtained after averaging four images and enforcing *c*12 symmetry. The unit cell is outlined and the location of the symmetry axis the marked. Solid contours represent stain-excluding regions, and dotted contours represent regions of stain accumulation.

either by dialysis or by successive additions of very small amounts of beads, led to a large increase in the stacking of 2D layers. Very large 3D crystals of Ca-ATPase were observed, similar to those obtained in the presence of detergent and at a higher lipid-to-protein ratio, 0.5 w/w (Dux et al., 1987; Stokes and Green, 1990a; Cheong et al., 1996). Second, intermediate rates of detergent removal, between slow and fast conditions, significantly reduced the size and the stacking of the wormlike multilamellar crystals as compared with the slow rates. In addition, coexisting with these wormlike crystals, tubular and even fused tubular crystals were also observed. Their main characteristic was a clear multilamellar stacking (two to five layers) as compared with the fast rates (Fig. 6).

Effects of medium composition on the crystallization process

We have studied some parameters that are reported as essential for the 3D crystallization of the Ca-ATPase (Taylor et al., 1988) and that might affect the 2D crystal packing.

We have observed that tubular and multilamellar crystal formation has the same calcium requirement as the 3D multilayer crystals obtained in the presence of detergent (Taylor et al., 1988). If EGTA is added to preformed crystals to reduce the free calcium concentration below the affinity of calcium transport sites, the periodicity within the crystal disappears within a few minutes, even if the overall shape is still observable. After some hours, the crystal shape

TABLE 3 Crystallization results upon fast rate of detergent removal

	—	Strings	Long strings	Tubular crystals	Tubular crystals	Vesicles	Vesicles	Vesicles
Final lipid-to-protein ratio by weight	0.05	0.10	0.15	0.20	0.25	0.45	0.85	1.85

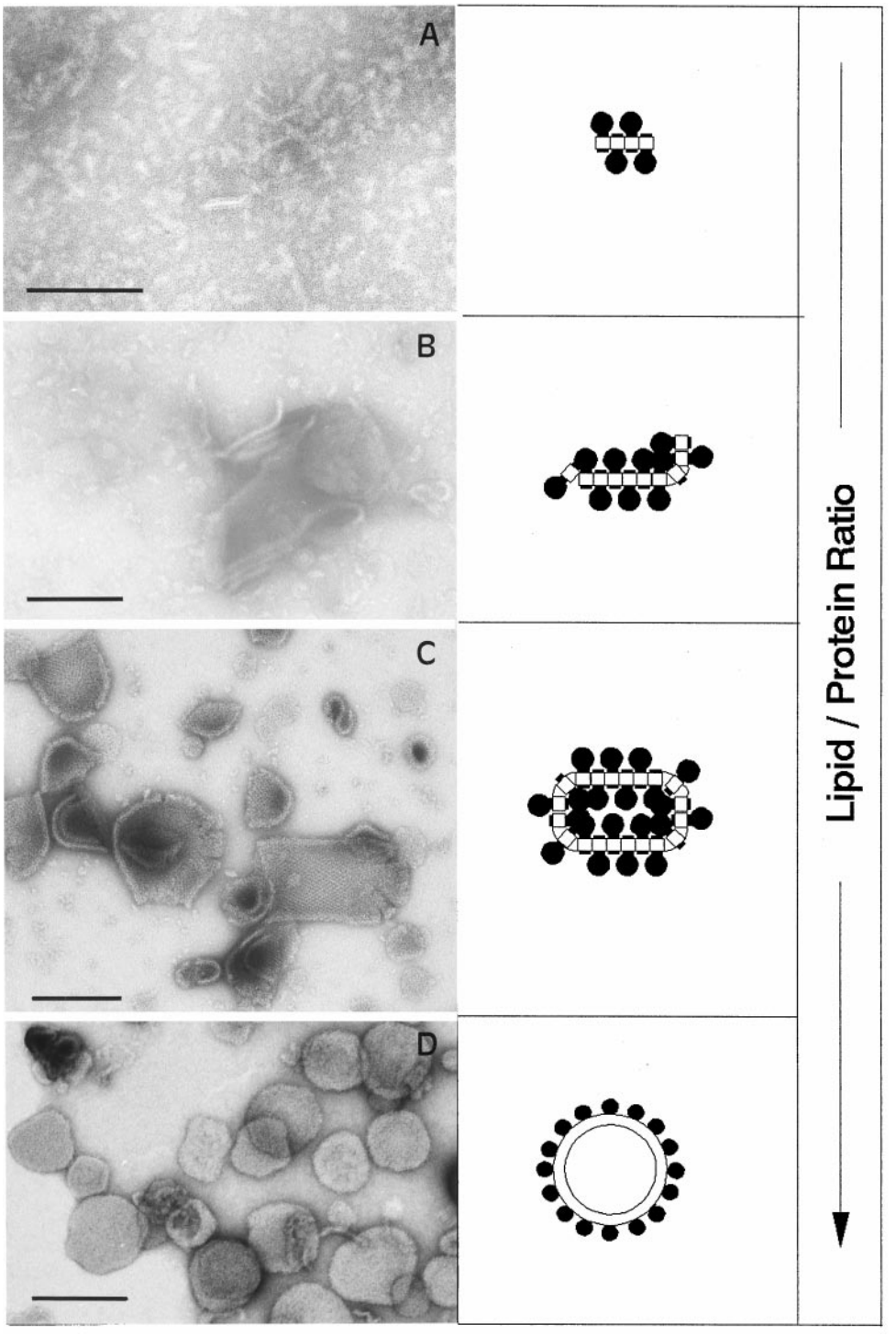

FIGURE 4 Effect of lipid-to-protein ratio on Ca-ATPase crystallization induced by a fast rate of detergent removal. The experimental conditions are as described in Fig. 2, except that C_{12E8} was removed by one addition of beads at a beads-to-detergent ratio of 40 w/w, corresponding to fast detergent removal as described in Fig. 1. Electron micrographs of samples reconstituted at different lipid-to-protein ratios: (*A*) Addition of 0.05 mg lipids per mg protein, i.e., final lipid/protein ratio = 0.10 w/w, taking into account the endogenous lipid in the purified Ca-ATPase. (*B*) Addition of 0.10 mg lipids per mg protein, i.e., final lipid/protein ratio = 0.15 w/w. (*C*) Addition of 0.15 mg lipids per mg protein, i.e., final lipid/protein ratio = 0.2 w/w. (*D*) Addition of 0.50 mg lipids per mg protein, i.e., final lipid/protein ratio = 0.55 w/w. Scale bar represents 200 nm.

completely disappears. If EGTA is added to the incubation medium before detergent removal, no crystals can be produced, whatever the rate of detergent removal. The calcium concentration required to get crystals after complete detergent removal with Bio-Beads is in the range of 0.1–0.2 mM, a concentration classically used to achieve saturation of the calcium transport sites in binding experiments (Forge et al., 1993). This is similar to the minimum Ca concentration required in the crystallization protocol for 3D crystals (Stokes and Lacapère, 1994), although a 10 mM concentration is generally used, because of the concomitant increase in protein stability (Pikula et al., 1988).

We have also observed that the presence of 5–20% glycerol or 1–10 mM magnesium does not change the shape and size of tubular and platelike crystals, in agreement with previous reports on crystals formed in the presence of detergent (Taylor et al., 1988; Shi et al., 1995). Tubular crystals are formed at pH 6 and 7 but not at pH 8 (data not

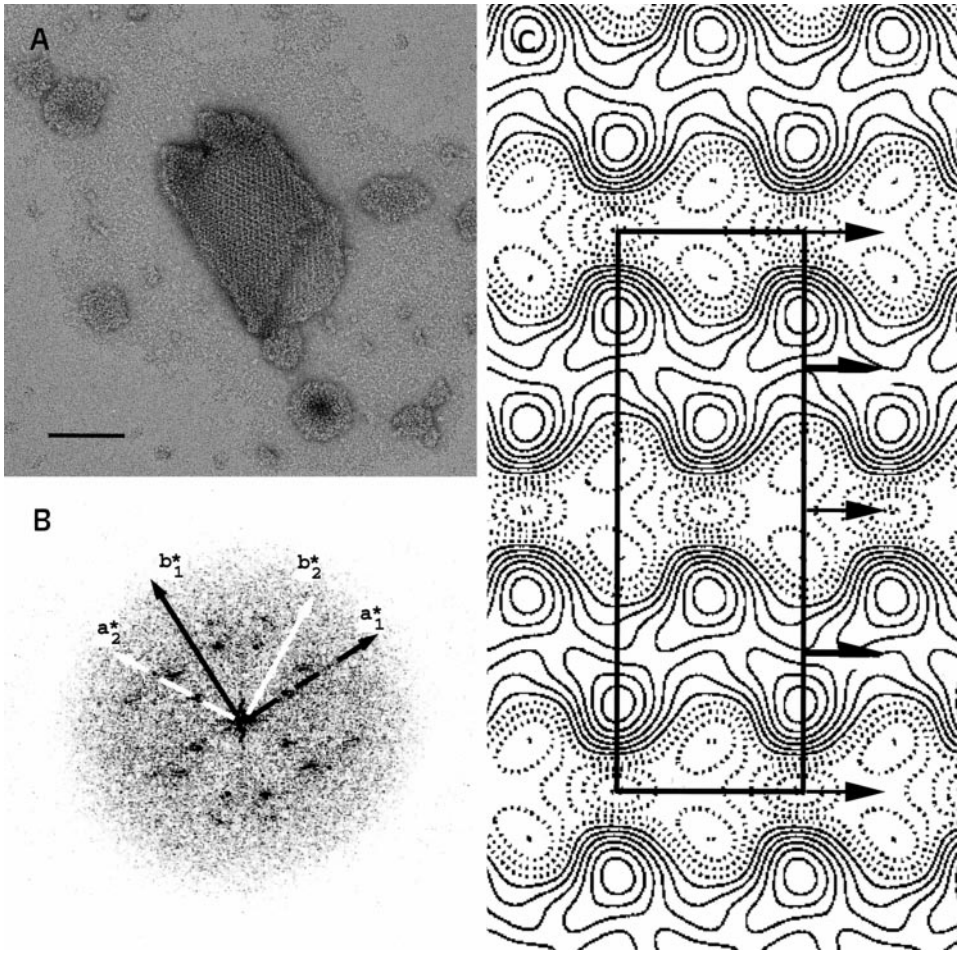

FIGURE 5 Image analysis of tubular Ca-ATPase crystals produced by a fast rate of detergent removal. (*A*) Negatively stained Ca-ATPase crystals (lipid/protein ratio = 0.2 w/w) recorded at high magnification. Scale bar represents 100 nm. (*B*) Computed diffraction pattern of Ca-ATPase crystals obtained by fast detergent removal. (*C*) Projection map of tubular crystals obtained after averaging 15 images from nine crystals and enforcing the *c*12 symmetry. Solid contours represent stain-excluding regions, and dotted contours represent regions of stain accumulation.

shown), exhibiting a less strict pH dependence than the multilamellar crystals formed in the presence of detergent, for which optimal conditions were reported at pH 6 (Taylor et al., 1988), with smaller crystals growing at pH 6.5 (Stokes and Green, 1990a).

Then we checked the effect of ADP, which is known to change protein conformation (Lacapère et al., 1990) and to prevent 3D multilamellar crystal formation in the presence of detergent (Stokes and Lacapère, 1994). Usually the tenfold dilution of purified Ca-ATPase (eluted from the column in ADP) in the crystallization medium reduces the ADP concentration to levels low enough to produce the multilamellar and tubular crystals previously described in Figs. 3 and 5. The addition of a millimolar ADP concentration to these preformed crystals induces a significant disruption of the crystals, and small patches of a different

TABLE 4 Determination of projection symmetry with ALLSPACE

Plane group	Multilayered	Tube	ADP
p1	25.0 ± 5	34.2 ± 4	24.0 ± 5
p2	44.4 ± 5	46.9 ± 10	33.0 ± 10
c12	22.0 ± 8 (10)	31.0 ± 10 (13)	13.0 ± 10 (10)
c222	43.0 ± 10	46.9 ± 10	36.0 ± 10

The phase residual (mean ± SD) represents comparison of symmetry-related reflections from five, nine, and seven individual images of multilayered, tubular, and ADP-induced crystals, respectively. In the case of p1 symmetry, the phase residuals are expectations based on the signal-to-noise ratio of reflections. For the c12 symmetry, the phase residuals for merging are shown in parentheses.

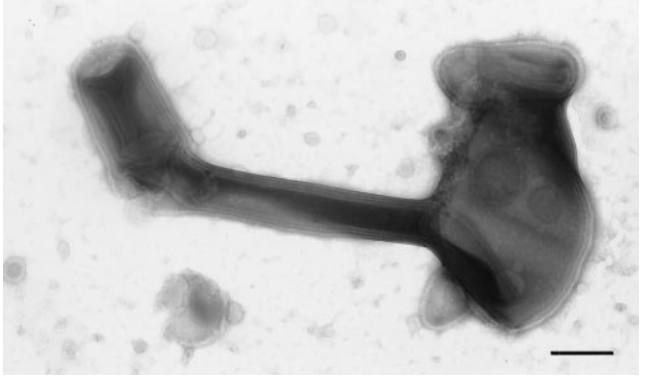

FIGURE 6 Multilamellar tubes of Ca-ATPase. Ca-ATPase crystals were induced at an intermediate rate of detergent removal. The experimental conditions are as described in Fig. 2, except that $C_{12}E_8$ was removed by two successive additions of beads with a bead/detergent ratio of 20 w/w. This electron micrograph of the sample was reconstituted at a final lipid-to-protein ratio of 0.15 w/w. The scale bar represents 200 nm.

crystal form can be observed. This new crystal form can also be obtained by adding 1–2 mM ADP before detergent removal. Fig. 7, *A* and *B*, shows such crystals obtained after fast and slow detergent removal, respectively. In contrast to the results in the absence of ADP, the morphologies of the 2D crystals produced in the presence of ADP were independent of the rate of detergent removal and were always single-layered. Importantly, upon slow detergent removal, no multilamellar stacking was detectable, and only small 2D crystals were produced. The protein orientation in the bilayer of these ADP-induced crystals appears to be bidirectional, with proteins protruding from both faces of the membrane. This is clearly shown at very low lipid-to-protein ratios (0.1–0.15 w/w), where we observed, after fast detergent removal, small strings containing a few protein molecules facing both sides of the bilayer (Fig. 7 *A*, *inset*). This is supported by the symmetry observed in projection. In particular, filtered images of such crystals (Fig. 7 *B*, *inset*) exhibit a packing of proteins along parallel and perpendicular rows. A typical computed diffraction pattern of these crystals is shown in Fig. 7 *C*, with clear spots for the first order at a resolution of 80 Å. After analysis of 15 crystals, the average unit cell parameters for these ADP-induced crystals are $a = 86 \pm 6$ Å, $b = 77 \pm 6$ Å, and $\gamma = 90 \pm 7°$. Examination of the phase residual indicated a *c*12 two-sided plane group (see Table 4). We get a 20-Å resolution projection map shown in Fig. 7 *D*. The molecules are clearly aligned along rows, and the mirror symmetry (*c*12) implies that proteins protrude on both sides of the membrane.

DISCUSSION

The results obtained from our systematic analysis of Ca-ATPase crystallization suggest a possible model of crystallogenesis (Fig. 8) that may be generally true for asymmetrical membrane protein with a large hydrophilic cytoplasmic domain.

This model takes into account the main observations of this work: 1) the bipolar orientation of the protein in the 2D crystals produced at lipid-to-protein ratios below 0.4 w/w; 2) the dependence of crystal morphology upon the rates of detergent removal; 3) the role of protein conformation in determining crystal packing.

Lipid-to-protein ratio

In the first place, protein insertion and the ultimate protein orientation within the bilayers appears to be governed by the initial lipid-to-protein ratio during detergent-mediated re-

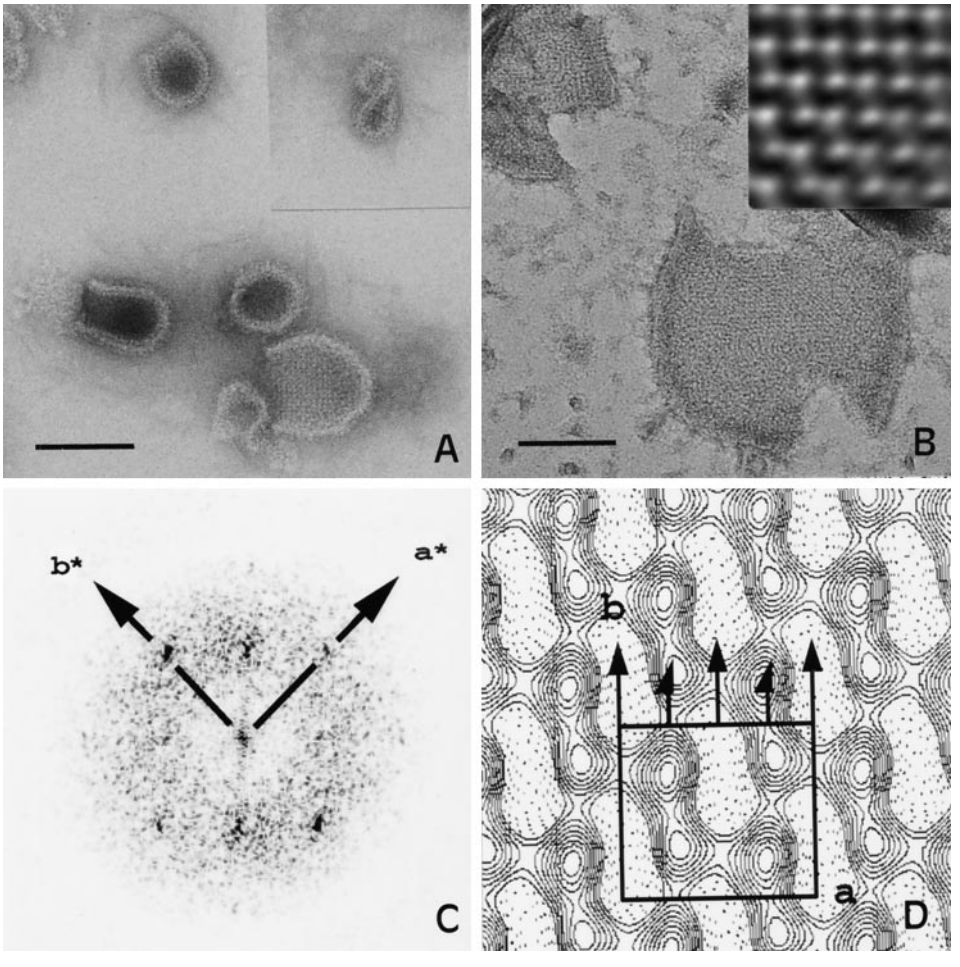

FIGURE 7 Ca-ATPase crystallization in the presence of ADP. The experimental conditions are as described in Fig. 2, except that 2 mM ADP was present in the incubation medium before detergent removal. $C_{12}E_8$ was removed according to Fig. 1 for slow and fast detergent removal, respectively. The final lipid-to-protein ratio was 0.25 w/w. (*A*) Electron micrograph of 2D crystals formed after fast detergent removal; the scale bar represents 100 nm. *Inset*: String formed at a lipid/protein ratio = 0.15 w/w. (*B*) Electron micrograph of 2D crystals formed after slow detergent; the scale bar represents 100 nm. *Inset*: Filtered image of crystal. (*C*) Computed diffraction pattern of Ca-ATPase crystals obtained in the presence of ADP. (*D*) The projection map was obtained after averaging three images. Solid contours represent stain-excluding regions, and dotted contours represent regions of stain accumulation.

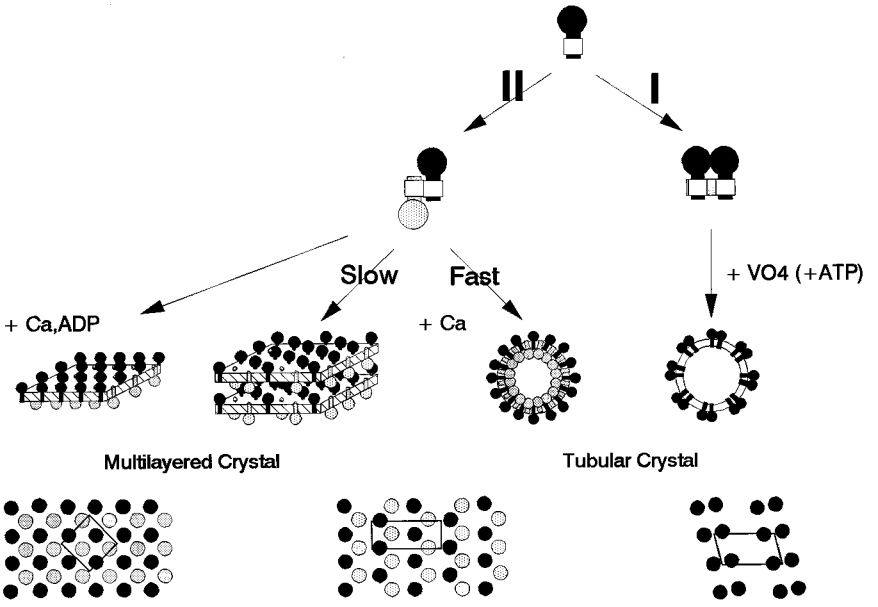

FIGURE 8 Schematic representation of Ca-ATPase 2D crystallization as a function of lipid-to-protein ratio, rate of detergent removal, and protein conformation.

constitutions of Ca-ATPase. At low lipid-to-protein ratios (below 0.4 w/w), 2D crystals are produced (*II* in Fig. 8). Although the size, shape, and morphology of these 2D crystals depend upon the rate of detergent removal and the protein conformation, in all cases, the large cytoplamic domains protude symmetrically from both sides of the bilayer. This is manifested as mirror symmetry in the projection images that we analyzed. At lipid-to-protein ratios above 0.4 (w/w), only noncrystalline proteoliposomes are formed (*I* in Fig. 8). In a recent study on the reconstitution of $C_{12}E_8$-solubilized Ca-ATPase into proteoliposomes at lipid-to-protein ratios between 0.5 and 2 (w/w), protein orientation was demonstrated to be mainly unidirectional, with the hydrophilic cytoplasmic domain of the protein facing the outside of the vesicles. Importantly, this asymmetry led to the ready formation of tubular crystals upon vanadate addition (Young et al., 1997).

Although we have no conclusive explanation for the dependence of protein sidedness on the initial lipid-to-protein ratio, two hypotheses can be advanced. The first is that when mixed micelles fuse and coalesce at the early stage of decreased detergent concentrations, specific hydrophobic protein-protein interactions predominate within the bilayer at low lipid-to-protein ratios. Ca-ATPase molecules, therefore, tend to interact through their transmembrane sectors, leading to a final up-and-down orientation in a bilayer. At high lipid-to-protein ratios, lipid-protein interactions might overcome protein-protein interactions within the bilayer. Under these conditions, the proteins are more likely to adopt a unidirectionnal orientation during micelle coalescence.

Our second hypothesis involves specific hydrophilic protein-protein interactions within the large hydrophilic domains. According to this hypothesis, bipolar Ca-ATPase orientation would be required to minimize the hydrophobic surface of the protein to be covered by the small amounts of lipid or detergent present at low lipid-to-protein ratios (a lipid-to-protein ratio of 0.25 w/w corresponds to only 35 lipid molecules per ATPase). Indeed, in a coalescent micelle or in a detergent-saturated bilayer, if two proteins interact through their large cytoplasmic parts, they leave large sectors of their transmembrane hydrophobic segments uncovered by detergents or lipids The only way to shield these large hydrophobic sectors from contact with the solvent would be the insertion of a Ca-ATPase molecule in the reverse direction. Upon increasing lipid-to-protein ratios, there is an excess of lipids to fill the space between two interacting proteins in the same orientation and minimize the hydrophobic surface. Consequently, the proteins could and would likely adopt a preferred asymmetrical orientation during the coalescence of mixed micelles or bilayer formation.

Speed of detergent removal

Our data demonstrate that the rate of detergent removal is an important parameter in the growth of 2D crystals. Comparison of fast and slow $C_{12}E_8$ removal indicates that slow detergent removal induced the formation of multilamellar crystals, whereas fast detergent removal induced the formation of linear arrays whose growth is limited to one dimension, and ultimately produced unilamellar tubular crystals.

According to a model proposed by Lasic (1988) for vesicle formation by detergent depletion techniques, three steps occur in the overall process of micellar-to-lamellar transformation: 1) micellar equilibration, including micellar growth by coalescence and fusion; 2) vesiculation (bilayer closure); and 3) postvesiculation growth. The basic concepts are that as detergent molecules are removed from micellar solutions, a series of micelle-micelle interactions is initiated, resulting in large disklike mixed micelles whose edges are coated with detergent. When they have grown past a critical radius, a subsequent bending of these large mi-

celles gives rise to curved detergent-saturated bilayers, followed, upon further detergent removal, by bilayer closure. These detergent-saturated bilayers (liposomes, proteoliposomes, or 2D crystals) are still capable of the phase transformation process (fusion or crystal growth) as long as the level of residual detergent remains high. This model predicts that slower detergent removal will produce larger bilayered structures, because there will be more time for micelle fusion and postvesiculation growth. This is consistent with current crystallization results and previous results from detergent-mediated reconstitution that have shown liposome or proteoliposome sizes decreased significantly upon fast detergent removal (Levy et al., 1990a,b; Young et al., 1997).

Interestingly, our results clearly demonstrate that multilayer stacking of planar 2D crystals is only observed upon slow detergent removal. This stacking appears to involve interactions between the exposed hydrophilic headgroups of ATPase molecules. In the case of fast detergent removal, these interactions have no time to develop, and single-layered structures are formed. Furthermore, a longer incubation after detergent removal did not result in stacking, suggesting that the relevant protein-protein interactions between layers only occur in the presence of detergent. There are two possible explanations for this dependence on detergent: 1) optimal interactions between the large hydrophilic domains of Ca-ATPases might require increased bilayer fluidity, as produced by detergent, which would, for example, increase the segmental and translational motion of ATPase molecules; 2) detergent might bind directly to the protein, thus stabilizing a particular conformation. In this regard, it should be noted that interaction between detergent headgroup and polar amino acid residues of Ca-ATPase is likely at the hydrophobic/hydrophilic interface, as indicated by the crucial importance of the detergent hydrophilic headgroup for maintaining activity and by the pH specificity of detergent-induced inactivation (Lund et al., 1989; Møller and Le Maire, 1993). The possibility of a detergent-induced conformation stabilizing the crystal form is reminiscent of the observed effect of ADP on 2D crystallization, which prevents the multilamellar stacking and produces a completely different 2D crystal form.

Protein conformation

Another important observation of this work is that the nucleation point for crystal formation is affected by the protein conformation. In our case, the tubular and multilayered crystals both required the presence of submillimolar calcium concentration, which imposes a particular conformation by saturating the calcium transport sites. Calcium removal either disrupts the preformed crystals or prevents crystal formation altogether. In addition, binding of ADP to the catalytic site gives rise to another type of packing of the Ca-ATPase within the unit cell (see Fig. 7), yet generally maintains the bipolar orientation of the molecule within the bilayer. These results are important with regard to the major unresolved question of the mechanism of coupling between calcium transport and ATP hydrolysis by Ca-ATPase. A first step will be to solve the three-dimensional structure of the protein in any conformation, but a second step would be to understand the conformational changes associated with the catalytic cycle. In this respect, 3D reconstruction from our 2D tubular crystals, with saturated calcium transport sites, should be compared with the structure deduced from vanadate-induced tubular crystals (Toyoshima et al., 1993), where the protein conformation requires empty calcium transport sites. Moreover, our new ADP-induced crystals in the presence of calcium provide an opportunity for yet another conformation of the Ca-ATPase, which should be compared with the recent structure described by Yonekura et al. (1997), in which an ATP analogue was bound in the absence of calcium.

CONCLUSION

In the current work, two-dimensional crystals of Ca-ATPase have been produced by complete detergent removal and without the need for chemical agents to induce crystallization. A major benefit of our method is the use of Bio-Beads to remove detergent. These Bio-Beads not only allow fast and total removal of the low critical micelle concentration detergent $C_{12}E_8$, but also allow control of the rate of detergent removal. As a result, our results provide some information about the mechanism of Ca-ATPase crystal formation. In addition, the tubular 2D crystals obtained upon fast detergent removal, as well as the unilamellar 2D sheets obtained in the presence of ADP, represent novel Ca-ATPase 2D crystals. It is possible that making these crystals larger and/or better ordered would provide an opportunity for even higher resolution structures of Ca-ATPase. In any case, the principles developed in this work are relevant to other membrane proteins (Rigaud et al., 1997; Lacapère et al., 1997) and, in particular, to the other members of the P-type ion pump family that are related in structure and function to Ca-ATPase. In this context, vanadate and phospholipase A2-induced 2D crystals of Na,K-ATPase, H,K-ATPase, and Kdp-ATPase have already been obtained in native membranes (Hebert et al., 1985; Mohraz et al., 1985; Iwane et al., 1996; Xian and Hebert, 1997), but are poorly ordered. Future structural analysis of these P-type ATPases will require crystallization by reconstitution from detergent-solubilized protein.

This work was partly funded by a European Economic Community grant (PL962119) to J-LR and National Institutes of Health grants (HL48807 and AR40997) to DLS.

REFERENCES

Champeil, P., G. Guillain, C. Venien, and M. P. Gingold. 1985. Interaction of magnesium and inorganic phosphate with calcium-deprived sarco-

plasmic reticulum adenosinetriphosphatase as reflected by inorganic solvent induced perturbation. *Biochemistry.* 24:69–81.

Cheong, G.-W., H. S. Young, H. Ogawa, C. Toyoshima, and D. L. Stokes. 1996. Lamellar stacking in the three-dimensional crystals of Ca^{2+}-ATPase from sarcoplasmic reticulum. *Biophys. J.* 70:1689–1699.

Dolder, M., A. Engel, and M. Zulauf. 1996. The micelle to vesicle transition of lipids and detergents in the presence of a membrane protein: towards a rationale for 2D crystallization. *FEBS Lett.* 382:203–208.

Dux, L., and A. Martonosi. 1983. Two-dimensional arrays of proteins in sarcoplasmic reticulum and purified Ca^{2+}-ATPase vesicles treated with vanadate. *J. Biol. Chem.* 258:2599–2603.

Dux, L., S. Pikula, N. Mullner, and A. Martonosi. 1987. Crystallization of Ca^{2+}-ATPase in detergent-solubilized sarcoplasmic reticulum. *J. Biol. Chem.* 262:6439–6442.

Dux, L., K. Taylor, H. P. Ting-Beall, and A. Martonosi. 1985. Crystallization of the Ca^{2+}-ATPase of sarcoplamic reticulum by calcium and lanthanide ions. *J. Biol. Chem.* 260:11730–11743.

Forge, V., E. Mintz, and F. Guillain. 1993. Ca^{2+} binding to sarcoplasmic reticuluml ATPase revisited. Mechanism of affinity and cooperativity modulation by H^+ and Mg^{2+}. *J. Biol. Chem.* 268:10953–10960.

Hao, L., J. L. Rigaud, and G. Inesi. 1994. Ca^{++}/H^+ countertransport and electrogenicity in proteoliposomes containing erythrocyte plasma membrane Ca-ATPase and exogeneous lipids. *J. Biol. Chem.* 269: 14268–14275.

Hebert, H., E. Skriver, and A. B. Maunsbach. 1985. Three-dimensional structure of renal Na,K-ATPase determined from two-dimensional membrane crystals of the p_1 form. *FEBS Lett.* 187:182–186.

Henderson, R., J. M. Baldwin, K. Downing, J. Lepault, and F. Zemlin. 1986. Structure of purple membrane from *Halobacterium halobium*: recording, measurements and evaluation of electron micrographs at 3.5 Å resolution. *Ultramicroscopy.* 19:147–178.

Iwane, A. H., I. Ikeda, Y. Kimura, Y. Fujiyoshi, K. Altendorf, and W. Epstein. 1996. Two-dimensional crystals of the Kdp-ATPase of *Echerichia coli. FEBS Lett.* 396:172–176.

Lacapère, J.-J., N. Bennett, Y. Dupont, and F. Guillain. 1990. pH and magnesium dependence of ATP binding to sarcoplasmic reticulum ATPase. *J. Biol. Chem.* 265:348–353.

Lacapère, J.-J., D. L. Stokes, G. Mosser, J.-L. Ranck, A. Olofsson, and J.-L. Rigaud. 1997. Two-dimensional crystals formation from solubilized membrane proteins using Bio-Beads to remove detergent. *Ann. N. Y. Acad. Sci.* 834:9–19.

Lasic, D. D. 1988. The mechanism of vesicle formation. *Biochem. J.* 256:1–11.

Levy, D., A. Bluzat, M. Seigneuret, and J. L. Rigaud. 1990a. A systematic study of liposome and proteoliposome reconstitution involving Bio-Bead-mediated Triton X-100 removal. *Biochim. Biophys. Acta.* 1025: 179–190.

Levy, D., A. Gulik, A. Bluzat, and J.-L. Rigaud. 1992. Reconstitution of the sarcoplasmic reticulum Ca^{2+}-ATPase: mechanisms of membrane protein insertion into liposomes during reconstitution procedures involving detergents. *Biochim. Biophys. Acta.* 1107:283–298.

Levy, D., A. Gulik, M. Seigneuret, and J.-L. Rigaud. 1990b. Phospholipid vesicle solubilization and reconstitution by detergents. Symmetrical analysis of the two processes using octaethylenee glycol mono-*n*-dodecyl ether. *Biochemistry.* 29:480–9488.

Levy, D., M. Seigneuret, A. Bluzat, and J.-L. Rigaud. 1990c. Evidence for proton countertransport by the sarcoplasmic reticulum Ca^{2+}-ATPase during calcium transport in reconstituted proteoliposomes with "low" ionic permeability. *J. Biol. Chem.* 265:19524–19534.

Lund, S., S. Orlovski, B. de Foresta, P. Champeil, M. Le Maire, and J. V. Møller. 1989. Detergent structure and associated lipid as determinants in the stabilization of solubilized Ca-ATPase from sarcoplasmic reticulum. *J. Biol. Chem.* 264:4907–4915.

Lutsenko, S., and J. H. Kaplan. 1995. Organisation of P-type ATPases: significance of structural diversity. *Biochemistry.* 48:15607–15613.

Misra, M., D. Taylor, T. Oliver, and K. Taylor. 1991. Effect of inorganic anions on the crystallization of the Ca^{2+}-ATPase of muscle sarcoplasmic reticulum. *Biochim. Biophys. Acta.* 1077:107–118.

Mohraz, M., M. Yee, and P. R. Smith. 1985. Novel crystalline sheets of Na,K-ATPase induced by phospholipase A_2. *J. Ultrastruct. Res.* 93: 17–26.

Møller, J. V., B. Juul, and M. Le Maire. 1996. Structural organization, ion transport, and energy transduction of P-type ATPases. *Biochim. Biophys. Acta.* 1286:1–51.

Møller, J. V., and M. Le Maire. 1993. Detergent binding as a measure of hydrophobic surface area of integral membrane proteins. *J. Biol. Chem.* 268:18659–18672.

Pikula, S., N. Mullner, L. Dux, and A. Martonosi. 1988. Stabilization and crystallization of Ca^{2+}-ATPase in detergent-solubilized sarcoplasmic reticulum. *J. Biol. Chem.* 263:5277–5286.

Rigaud, J.-L., D. Levy, G. Mosser, and O. Lambert. 1998. Detergent removal by non-polar polystyrene beads. *Eur. Biophys. J.* 27:305–319.

Rigaud, J.-L., G. Mosser, J.-J. Lacapère, A. Olofsson, D. Levy, and J.-L. Ranck. 1997. Bio-beads: an efficient strategy for two-dimensional crystallization of membrane proteins. *J. Struct. Biol.* 118:226–235.

Rigaud, J.-L., B. Pitard, and D. Levy. 1995. Reconstitution of membrane proteins into liposomes: application to energy-transducing membrane proteins. *Biochim. Biophys. Acta.* 1231:223–246.

Rouser, G., S. Fleischer, and A. Yamamoto. 1970. Two dimensional thin layer chromatographic separation of polar lipids and determination of phospholipids by phosphorus analysis of spots. *Lipids.* 5:494–496.

Shi, D., H.-H. Hsiung, R. C. Pace, and D. L. Stokes. 1995. Preparation and analysis of large, flat crystals of Ca^{2+}-ATPase for electron crystallography. *Biophys. J.* 68:1152–1162.

Stokes, D. L. 1991. P-type ion pumps: structure determination may soon catch up with structure predictions. *Curr. Opin. Struct. Biol.* 1:555–561.

Stokes, D. L., and N. M. Green. 1990a. Three-dimensional crystals of Ca^{2+}-ATPase from sarcoplasmic reticulum: symmetry and molecular packing. *Biophys. J.* 57:1–14.

Stokes, D. L., and N. M. Green. 1990b. Structure of Ca^{2+}-ATPase: electron microscopy of frozen-hydrated crystals at 6 Å resolution in projection. *J. Mol. Biol.* 213:529–538.

Stokes, D. L., and J.-J. Lacapère. 1994. Conformation of Ca^{2+}-ATPase in two crystals forms: effects of Ca^{2+}, thapsigargin, AMP-PCP and Cr-ATP on crystallization. *J. Biol. Chem.* 269:11606–11613.

Taylor, K. A., N. Mullner, S. Pikula, L. Dux, C. Peracchia, S. Varga, and A. Martonosi. 1988. Electron microscope observations on Ca^{2+}-ATPase microcrystals in detergen-solubilized sarcoplasmic reticulum. *J. Biol. Chem.* 263:5287–5294.

Toyoshima, C., H. Sasabe, and D. L. Stokes. 1993. Three-dimensional cryo-electron microscopy of the calcium pump in the sarcoplasmic reticulum membrane. *Nature.* 362:469–471.

Valpuesta, J. M., J. L. Carrascosa, and R. Henderson. 1994. Analysis of electron microscopy images and electron diffraction patterns of thin crystals of ∅29 connectors in ice. *J. Mol. Biol.* 240:281–287.

Varga, S. 1994. Three-dimensional (type I) micocrystals of detergent-solubilized membrane-bound gastric (H^+,K^+)-ATPase from hog and rabbit stomachs. *Acta Physiol. Hung.* 82:365–376.

Varga, S., K. Taylor, and A. Martonosi. 1991. Effects of solutes on the formation of crystalline sheets of the Ca-ATPase in detergent-solubilized sarcoplasmic reticulum. *Biochim. Biophys. Acta.* 1070: 374–386.

Xian, Y., and H. Hebert. 1997. Three-dimensional struture of the porcine gastric H,K-ATPase from negatively stained crystals. *J. Struct. Biol.* 118:169–177.

Yonekura, K., D. L. Stokes, H. Sasabe, and C. Toyoshima. 1997. The ATP-binding site of Ca^{2+}-ATPase revealed by electron image analysis. *Biophys. J.* 71:997–1005.

Young, H. S., J.-L Rigaud, J.-J. Lacapère, L. G. Reddy, and D. L. Stokes. 1997. How to make tubular crystals by reconstitution of detergent-solubilized Ca^{2+}-ATPase. *Biophys. J.* 72:2545–2558.

Zhang, P., C. Toyoshima, K. Yonekura, N. M. Green, and D. L. Stokes 1998. Structure of the calcium pump from sarcoplasmic reticulum at 8-Å resolution. *Nature.* 392:835–839.